

# Critical growth of cerebral tissue in organoids: theory and experiments

Egor I. Kiselev,<sup>1,\*</sup> Florian Pflug,<sup>1,†</sup> and Arndt von Haeseler<sup>1,2</sup>

<sup>1</sup>Center for Integrative Bioinformatics Vienna (CIBIV), Max Perutz Laboratories, University of Vienna and Medical University of Vienna, Vienna Bio Center (VBC), Vienna, Austria

<sup>2</sup>Bioinformatics and Computational Biology, Faculty of Computer Science, University of Vienna, Vienna, Austria

We develop a Fokker-Planck theory of tissue growth with three types of cells (symmetrically dividing, asymmetrically dividing and non-dividing) as main agents to study the growth dynamics of human cerebral organoids. Fitting the theory to lineage tracing data obtained in next generation sequencing experiments, we show that the growth of cerebral organoids is a critical process. We derive analytical expressions describing the time evolution of clonal lineage sizes and show how power-law distributions arise in the limit of long times due to the vanishing of a characteristic growth scale.

*Introduction* The mechanisms of tissue growth and renewal are a core topic of stem-cell research [1, 2]. In particular, the role of stochasticity in cell differentiation is discussed [3–8]. Modern gene sequencing protocols – commonly referred to as next generation sequencing (NGS) – allow to study the genome of individual cells (single cell sequencing) [9]. In combination with the labeling of cells with inheritable DNA sequences, these techniques enable large scale, quantitative studies of cell populations in biological tissues, allowing to trace back offspring populations to their individual ancestral cells [10, 11]. Such lineage tracing experiments have revealed that offspring numbers in mammalian cerebral tissue can vary by several orders of magnitude [6, 12], which supports the hypothesis that stochasticity is an important property of cell proliferation and differentiation in the developing cerebral cortex.

This work presents a study of lineage tracing data obtained by sequencing 15 cerebral organoids at different stages of their development [12]. Cerebral organoids are highly controllable, self organized in vitro models of the human cerebral cortex grown directly from stem cells. Organoids are unique because they model human tissues which cannot be studied in vivo. They have therefore become important biological tools to study neural development and brain diseases [13–15]. While we focus on cerebral organoids, other types, such as retinal [16, 17], cardiac [18, 19] and intestinal [20, 21] organoids are widely studied. We take a physics point of view on the population dynamics of cell lineages in cerebral organoids, and show that organoid growth is a critical process and thus strong stochasticity resulting in power-law lineage size distributions is a core feature of the growth process.

*Model* Our study begins with the observation that the numbers of descendants of an individual stem cell

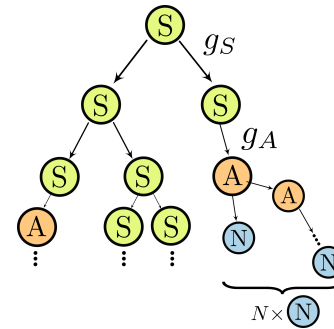


Figure 1. The SAN model of dividing and differentiating cells. Stem cells (green, S) maintain the potential for symmetric division ( $S \rightarrow 2S$ ) which happens at a rate  $g_S$ . Differentiated cells (orange and blue) either divide asymmetrically ( $A \rightarrow A+N$ ) with a rate  $g_A$  or lose this ability altogether (N). The growth process is driven by the while each asymmetrically dividing cell produces  $N$  N-cells on average, until it is terminated by a direct  $A \rightarrow N$  process. At criticality, the rates  $g_S$  (division) and  $g_A$  (differentiation) are equal.

in the organoid (lineage sizes) are roughly distributed according to a  $3/2$ -power-law (Fig. 2). This behavior becomes more and more pronounced at late stages of the organoid development. To study the growth process, we introduce the *SAN model*. It consists of three agents: symmetrically dividing S-cells that represent stem cells, asymmetrically dividing A-cells and non-dividing N-cells (fully developed cells, e.g. neurons). S-cells undergo symmetric division ( $S \rightarrow 2S$ ), differentiation ( $S \rightarrow A$ ) and death ( $S \rightarrow 0$ ). A-cells have committed to a developmental trajectory and produce N-cells through asymmetric divisions ( $A \rightarrow A+N$ ) until the process is terminated by direct differentiation ( $A \rightarrow N$ ) or death. The branching process of symmetric division and differentiation of S-cells with rates  $g_S$  and  $g_A$  is at the heart of the SAN-model. Criticality is reached, when the two rates are equal:  $g_S = g_A$ . The model is illustrated in Fig. 1. We solve the SAN-model analytically in the continuum limit and show how, at long times,  $3/2$ -power-law distributions of cell populations asymptotically arise near criticality. Fitting the model predictions to the empirical data of Ref. [12], we show that cerebral organoid growth is indeed critical (see

\* E.K. and F.P. contributed equally to this work; Current affiliation: Physics Department, Technion, 320003 Haifa, Israel; kiselev.physics@gmail.com

† E.K. and F.P. contributed equally to this work; Current affiliation: Biological Complexity Unit, Okinawa Institute of Science and Technology Graduate University, Onna, Okinawa 904-0495, Japan; florian.pflug@oist.jp

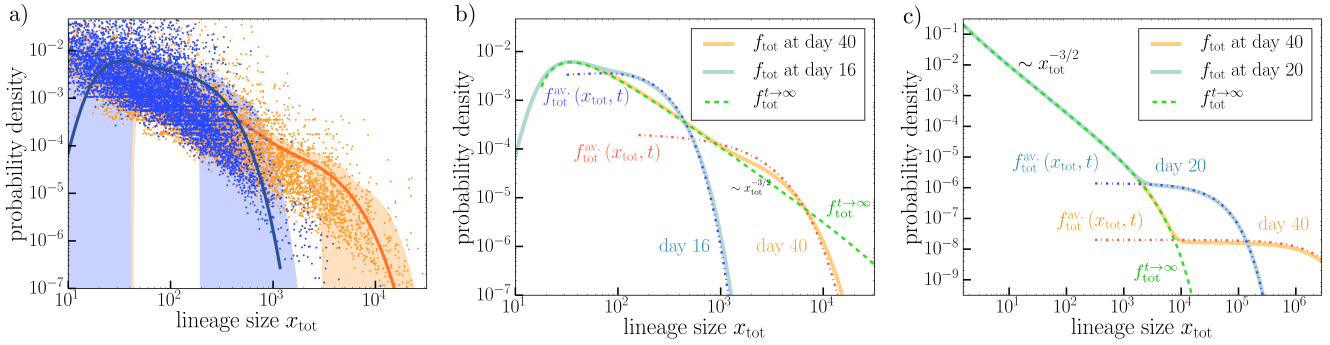


Figure 2. a) lineage size probability density of the SAN model  $f_{\text{tot}}(x_{\text{tot}}, t)$  (see subfigure b) for details) at  $t = 16$  days (blue solid line) and  $t = 40$  days (orange solid line) and the empirical probability densities at the same days (scattered points). The shown data is combined from six sequenced organoids (three per day). The estimates for the SAN parameters  $\alpha$  (net growth rate) and  $\beta$  (stochasticity rate) are given in Table I.  $f_{\text{tot}}(x_{\text{tot}}, t)$  was obtained using a Fast Fourier Transform (FFT) of the characteristic function of Eq. (S33). b) FFT-calculated SAN model probability densities from a) and the analytical approximations  $f_{\text{tot}}^{t \rightarrow \infty}(x_{\text{tot}})$  (dashed, green line) and  $f_{\text{tot}}^{\text{av}}(x_{\text{tot}}, t)$  (dashed, dotted lines) of Eqs. (5), (6) for the parameter estimates of Table I ( $\alpha < 0$ ). For  $t \rightarrow \infty$  the distribution approaches the weakly truncated  $3/2$ -power-law Lévy distribution  $f_{\text{tot}}^{t \rightarrow \infty}(x_{\text{tot}})$  everywhere. For small  $t$  there is a region where  $f_{\text{tot}}(x_{\text{tot}}, t)$  is well approximated by  $f_{\text{tot}}^{\text{av}}(x_{\text{tot}}, t)$  and exceeds  $f_{\text{tot}}^{t \rightarrow \infty}(x_{\text{tot}})$  before it quickly truncates. This region moves towards higher  $x_{\text{tot}}$  as  $t$  increases and marks the active part (avalanche part) of the population with actively dividing S-cells. Since the net S-cell growth rate  $\alpha$  is negative, this region becomes less and less pronounced for large  $t$ . The rates used in the plot are the same as in subfigure a). c) SAN model predictions for small  $\alpha > 0$ . The S-cell population proliferates indefinitely, however  $f_{\text{tot}}(x_{\text{tot}}, t)$  still approaches  $f_{\text{tot}}^{t \rightarrow \infty}(x_{\text{tot}})$ , except for very large lineage sizes. Here the probability distribution exceeds the  $t \rightarrow \infty$  limit. This region marks the avalanche regime of active S-cell proliferation for positive  $\alpha$ . We used  $\alpha = 0.2$ ,  $\beta = 10$ ,  $s_0 = 1$  and  $N = 1$ .

Fig. 2 and Table I).

In experiments, organoids are grown for forty days. As we will demonstrate, even at  $t = 40$  days the growth is not completed and the lineage distribution is far from its  $t \rightarrow \infty$  limit. It is therefore essential to obtain solutions that describe the organoids at finite times. In the following we show that our model is well suited to describe tissue growth as a dynamical process with only a limited number of parameters (three rates and one initial condition), allowing us to fit and model data throughout the growth process.

*Fokker-Planck description of lineage dynamics* Our mathematical approach to the SAN model of Fig. 1 is based on a multivariate Fokker-Planck Equation for the lineage size distribution. We begin by writing down a master equation for the SAN processes. We want to keep in mind that the individual populations of S, A and N-cells are not accessible in lineage tracing experiments, since all descendants of a given stem cell inherit the same lineage identifier. To compare our theory to experiments, we therefore need to calculate the probability distribution of the total lineage size  $x_{\text{tot}} = s + a + n$ . This becomes simpler if we slightly modify our model by replacing the processes that generate N-cells ( $A \rightarrow A + N$  and  $A \rightarrow N$ ) by simply assuming that each A-cell produces  $N = 1 + g_N/g_F$  N-cells over the course of its existence (where the +1 stems from the final  $A \rightarrow N$  conversion) (Fig. 1). Since the N-cell output per A-cell varies by multiple orders of magnitude less than the total offspring of each S-cell [22], this simplification does not affect the main predictions of the model, making it

analytically tractable. Below we denote this process as  $S \rightarrow (A) \rightarrow NN$ .  $N$  is a fitting parameter in our theory. The total lineage size becomes  $x_{\text{tot}} = s + n$ . With this assumption, the master equation for the probability distribution  $f$  of S- and N-cell numbers  $s, n$  at time  $t$  reads

$$\begin{aligned} \partial_t f(s, n, t) = & g_S (s - 1) f(s - 1, n, t) \\ & + g_A (s + 1) f(s + 1, n - N, t) \\ & + g_0 (s + 1) f(s + 1, n, t) \\ & - (g_S s + g_A s + g_0 s) f(s, n, t). \end{aligned} \quad (1)$$

The right hand side terms of Eq. (1) correspond to the different processes that the cells undergo: Each combination of cell numbers  $s, n$  represents a state which the system might occupy with the probability  $f(s, n, t)$ . The time derivative on the left hand side indicates that we are considering the rate of change of  $f(s, n, t)$ . The terms  $g_S (s - 1) f(s - 1, n, t)$  and  $-g_S s f(s, n, t)$  describe symmetric S-cell divisions at a rate  $g_S$ . Stem cell death is described by terms proportional to  $g_0$ . The second right hand side term accounts for an  $S \rightarrow (A) \rightarrow NN$  transition while the system is in a state with  $s + 1$  S-cells. The term  $-g_A s f(s, n, t)$  represents an  $S \rightarrow (A) \rightarrow NN$  process with the system being in a state with  $s$  S-cells. We translate the discrete process given by (1) into a continuous version given by the Fokker-Planck equation [23]:

$$\partial_t f(\mathbf{x}, t) = \mathcal{L} f(\mathbf{x}, t) \quad (2)$$

with the differential operator

$$\mathcal{L} = \left( -\alpha \partial_s + \frac{\beta}{2} \partial_s^2 - g_A N \partial_s \partial_n - N g_A \partial_n + \frac{g_A N^2}{2} \partial_n^2 \right) s. \quad (3)$$

Here,  $\mathbf{x} = (s, n)$  is a vector with the cell numbers as components,  $\alpha = g_S - g_A - g_0$  and  $\beta = g_S + g_A + g_0$ .  $s$  and  $n$  become continuous variables. For small  $s$  the results of the continuous and discrete approaches will differ, yet both are reasonable approximations of biological reality. While using the discrete version may seem preferential at first, cell division is only the end result of a series of changes to a cell's internal state as it transitions through the G1, S, G2 and M stages of the cell cycle. Because the continuous process accounts for these changes by allowing cell counts to change gradually, it may be in fact the model that is closer to reality.

*Regimes of growth: power-laws and avalanches* Next, we want to examine the implications of the Fokker-Planck Eq. (2) for the lineage sizes within a tissue sample. To this end we solve Eq. (2) with the initial condition  $f(\mathbf{x}, t=0) = \delta(s - s_0) \delta(n)$ .  $s_0$  corresponds to the initial number of stem cells of a lineage – not necessarily unity, since stem cells proliferate at initial stages of organoid preparation, which are not considered here otherwise. Using the Fourier transform of Eqs. (2), (3) with respect to  $\mathbf{x}$  and the method of characteristics to solve the resulting first order partial differential equation (see supplementary material), we find the characteristic function of  $f(\mathbf{x}, t)$ ,  $\tilde{f}(\mathbf{q}, t)$ , which is it's Fourier transform:  $\tilde{f}(\mathbf{q}, t) = \int_{-\infty}^{\infty} e^{-i\mathbf{q}\cdot\mathbf{x}} f(\mathbf{x}, t)$ .

Since experiments measure the total lineage size  $x_{\text{tot}} = s + n$  and not the individual cell numbers  $s$  and  $n$ , we are interested in the probability distribution for  $x_{\text{tot}}$ , which we call  $f_{\text{tot}}(x_{\text{tot}}, t)$ . This distribution is given by an integral of  $f(\mathbf{x}, t)$  over all states with equal  $x_{\text{tot}}$ :

$$f_{\text{tot}}(x_{\text{tot}}, t) = \int_0^{x_{\text{tot}}} f(s, x_{\text{tot}} - s, t) ds, \quad (4)$$

where  $f(\mathbf{x}, t)$  is the solution to Eq. (2).

We find that the behavior of  $f_{\text{tot}}$  qualitatively depends on the sign and value of the S-cell growth rate  $\alpha$ . For large times  $t \rightarrow \infty$ ,  $f_{\text{tot}}(x_{\text{tot}}, t)$  approaches a limiting distribution  $f_{\text{tot}}^{t \rightarrow \infty}(x_{\text{tot}})$ , which is a truncated 3/2-power-law:

$$f_{\text{tot}}^{t \rightarrow \infty}(x_{\text{tot}}) \approx \frac{s_0 \beta e^{-\frac{\alpha^2 x_{\text{tot}}}{\beta^2 N}}}{2\sqrt{2\pi} N (x_{\text{tot}}/N)^{3/2}}. \quad (5)$$

At criticality ( $\alpha = 0$ ), the exponential truncation vanishes, and the distribution becomes a true 3/2-power-law. For small  $|\alpha|$ , the truncation will only become important at very large  $x_{\text{tot}}/N > \beta^2/\alpha^2$ . In other words, the smaller the growth rate, the more pronounced the power-law.

The way in which  $f_{\text{tot}}(x_{\text{tot}}, t)$  approaches the limiting distribution of Eq. (5) is very different for  $\alpha > 0$  and

$\alpha < 0$ . For positive  $\alpha$ , for any finite  $t$  and large enough lineage size  $x_{\text{tot}} > x_{\text{tot}}^* \sim e^{\alpha t}$ , there is a regime where  $f_{\text{tot}}(x_{\text{tot}}, t)$  is not approximated by Eq. (5). This is the *avalanche regime* illustrated in Fig. 1. Here lineages have a high percentage of S-cells which are proliferating and driving the system towards larger lineage sizes, while for  $x_{\text{tot}} < x_{\text{tot}}^*$  most lineages are fully differentiated and do not grow any more. While the size of lineages in the avalanche regime can become very large, the probability with which such large lineage sizes occur becomes smaller and smaller. This behavior is illustrated in Fig. (2) c). In the avalanche regime,  $f_{\text{tot}}(x_{\text{tot}}, t)$  can be approximated by

$$f_{\text{tot}}^{\text{av.}}(x_{\text{tot}}, t) \approx \frac{\sqrt{a} \exp\left(-\frac{a}{q_{\text{tot}}^*} - \frac{x_{\text{tot}}}{q_{\text{tot}}^* N}\right)}{q_{\text{tot}}^* \sqrt{x_{\text{tot}} N}} I_1\left(2\sqrt{\frac{a x_{\text{tot}}}{q_{\text{tot}}^* N}}\right) \quad (6)$$

where  $I_1(z)$  is the modified Bessel function of the first kind and  $q_{\text{tot}}^*(t)$  and  $a(t)$  are non trivial time dependent coefficients which are defined in [supplementary Eqs. \(S 37\) and \(S 42\)](#). These results are derived in the supplementary material.

For a negative  $\alpha$ , we also find an avalanche regime hosting an active S-cell population (even though the avalanche will stop eventually). This regime is located at large  $x_{\text{tot}}$ , and is marked by a region where  $f_{\text{tot}}(x_{\text{tot}}, t)$  is larger than the limiting distribution  $f_{\text{tot}}^{t \rightarrow \infty}(x_{\text{tot}})$ , followed by a rapid truncation at even larger  $x_{\text{tot}}$  (Fig. 2 b)). In contrast to the behavior at  $\alpha > 0$ ,  $f_{\text{tot}}(x_{\text{tot}}, t)$  converges to  $f_{\text{tot}}^{t \rightarrow \infty}(x_{\text{tot}})$  uniformly, i.e. avalanches becomes less and less pronounced as  $t \rightarrow \infty$ . This is related to the fact that all lineages eventually die out if  $\alpha \leq 0$  [24]. Our estimates show, that  $\alpha \lesssim 0$  holds in experiments (see Table I). The analytical approximation (6) holds for the avalanche part of the lineage size distribution for  $\alpha < 0$ , if  $t$  is sufficiently small, i.e.  $\alpha t \lesssim 1$ . In particular, it holds reasonably well for the experimental data, as we demonstrate in Fig. 2 b). This has to do with the analytical structure of the characteristic function  $\tilde{f}_{\text{tot}}(q_{\text{tot}}, t)$  which is discussed in the supplementary material.

*Dynamics and criticality in experiments* The experimental data consists of lineage identifier counts for 15 organoids that were sequenced on days 16, 21, 25, 32 and 40 – three copies for each day [12]. Accounting for statistical and readout errors, the lineage identifier counts can be related to lineage sizes, i.e. to the numbers of cells in each lineage [22]. The organoids grow undisturbed from day 11 onward, when they are not subjected to intrusive procedures anymore. In our model, four parameters are determined from experimental data:  $\alpha$  – the net growth rate of the S-cell population,  $\beta$ , measuring the stochasticity of the process,  $s_0$  – the average stem cell population per lineage at day 11 and  $N$  – the number of N-cells that are produced by each asymmetrically dividing A-cell. The data at day 40 is very roughly distributed according to an  $x^{-3/2}$  power-law (see Fig. 2). Therefore, we can assume that we are near criticality and  $\alpha \ll \beta$

$\alpha$ [day <sup>-1</sup> ]	$-0.018 \pm 0.004$
$\beta$ [day <sup>-1</sup> ]	$4 \pm 1$
$s_0$	$9 \pm 3$
$N$	$2 \pm 1$

Table I. Parameters of the SAN model estimated from experimental data with one standard deviation errors.  $\alpha$  is the net growth rate of the stem cell population. The small value of  $\alpha$  as compared to the stochasticity rate  $\beta$  indicates that the system is close to criticality.  $s_0$  and  $N$  are the average initial number of stem cells and the average number of N-cells produced by each stem cell, respectively.

holds. To determine the parameters precisely, we use the empirical characteristic function of the data

$$\tilde{f}_{\text{exp}}(q_{\text{tot}}) = \sum_k e^{iq_{\text{tot}}x_{\text{tot}}^{(k)}}. \quad (7)$$

Here  $x_{\text{tot}}^{(i)}$  are the experimentally determined lineage sizes. The characteristic function of our model  $\tilde{f}(q_{\text{tot}}, t)$  (see Eq. (S33)) is then least squares fitted to  $\tilde{f}_{\text{exp}}(q_{\text{tot}})$ . Moving the fitting procedure to Fourier space has several advantages:  $\tilde{f}_{\text{exp}}(q_{\text{tot}})$  is less noisy than the empirical probability distribution and no smoothing procedures such as kernel density estimates need to be used. Finally approximations that are needed when transforming  $\tilde{f}(q_{\text{tot}}, t)$  to real space are avoided. Our estimates for the model parameters are shown in Table I. It is interesting to visualize the estimates obtained by fitting the characteristic functions in terms of probability densities. In Fig. 2 a) we show a comparison between the probability densities of the SAN model  $f_{\text{tot}}(x_{\text{tot}}, t)$  and the empirical probability densities at days 16 and 40. The empirical probability densities are obtained by taking the discrete derivatives of the cumulative probability distributions

$$p(x_{\text{tot}}) = \frac{1}{N} \sum_i \Theta(x_{\text{tot}} - x_{\text{tot}}^{(i)}), \quad (8)$$

where  $N$  is the total number of data points  $x_{\text{tot}}^{(i)}$  and  $\Theta(x_{\text{tot}})$  is the Heaviside theta function with  $\Theta(0) = 1$ .  $f_{\text{tot}}(x_{\text{tot}}, t)$  is found using a Fast Fourier Transform of the characteristic function  $\tilde{f}(q_{\text{tot}}, t)$ .

The estimates of Table I show that organoid growth is indeed a self organized critical process with  $|\alpha| \ll \beta$ . It also shows that even at day 40 the process is far from its  $t \rightarrow \infty$  limit ( $\alpha t \approx 0.8$ ) and the organoids maintain an avalanche-like population of S-cells at large  $x_{\text{tot}}$ .

The *SAN model* is only a minimal model of biological reality and as such cannot account for the full spread of the experimental data. It does, for example, not account for the data at small  $x_{\text{tot}}$  (see Fig. 2). Many small lineages have died out in the early stages of the organoid development and are obviously not described by SAN dynamics. For the analytical results, we assumed that all lineages consist of  $s_0$  stem cells at day 11. This value

is only an average over the different lineages. While for the very large lineages the initial number of stem cells is not important since the growth is stochastic, it matters for lineages that differentiated quickly. Other neglected aspects are the time dependence of rates, and the non-markovian nature of division and differentiation. Despite these caveats, the *SAN model* proves to be surprisingly robust and fits the experimental data well.

*Extinction trajectories* We now turn to the influence of criticality on the dynamics of single lineages. We focus on  $\alpha = 0$  and restrict ourselves to S-cells as the only dynamical component. Neglecting the dynamics of the  $n$  variable, we drop all but the first two terms in  $\mathcal{L}$  in Eq. (3). This reduced Fokker-Planck equation is equivalent to the stochastic differential equation

$$ds = \sqrt{\beta s} dw(t), \quad (9)$$

which governs the dynamics of  $s$ .  $w(t)$  is the standard Brownian motion. It is known that any  $s(t)$  described by Eq. (9), at some time  $\tau$ , reaches  $s(\tau) = 0$  [24], i.e. the S-cell population of the lineage goes extinct due to differentiation. Using the Onsager-Machlup formalism and the variable transform  $y = 2\sqrt{s/\beta}$ , we find an action corresponding to equation of motion (9). Minimizing the action with the boundary conditions  $s(0) = s_0$  and  $s(\tau) = 0$ , we find the *extinction trajectory*

$$s_\tau(t) = s_0 \left(1 - \frac{t}{\tau}\right) \left(1 + \left(\frac{\tau}{\hat{\tau}} - 1\right) \frac{t}{\tau}\right), \quad (10)$$

which describes the most probable path between the two boundary conditions (see Fig. 3).  $\hat{\tau} = 4s_0/(\sqrt{3}\beta)$  Details of the calculation are given in the supplementary material. Eq. (10) and Fig 3 show that at criticality, the cells loose memory of the initial condition  $s_0$ , since for  $\hat{\tau} \ll t < \tau$

$$s_\tau(t) \sim \sqrt{3}\beta t(1 - t/\tau)/4. \quad (11)$$

This is not the case for  $\alpha \geq 0$ . Since S-cells produce A-cells at a constant rate  $g_A$ , the total lineage size can be estimated as

$$\ell(\tau) = Ng_A \int_0^\tau s_\tau(t) dt. \quad (12)$$

Most importantly, since the lineage sizes are power-law distributed, an overwhelming majority of organoid cells will belong to a few very large lineages. For this lineages,  $\tau \gg \hat{\tau}$  will hold, meaning that their development will be largely independent of the initial condition  $s_0$  according to Eqs. (11) and (12). This is an essential feature of critical growth: it is largely independent of the initial conditions.

*Discussion* Finally, we discuss possible implications of critical tissue growth. Tuning itself to the critical point, the organoid maximizes the stochasticity of the growth process. We are not dealing with stochastic growth at a given rate. Instead, the characteristic time

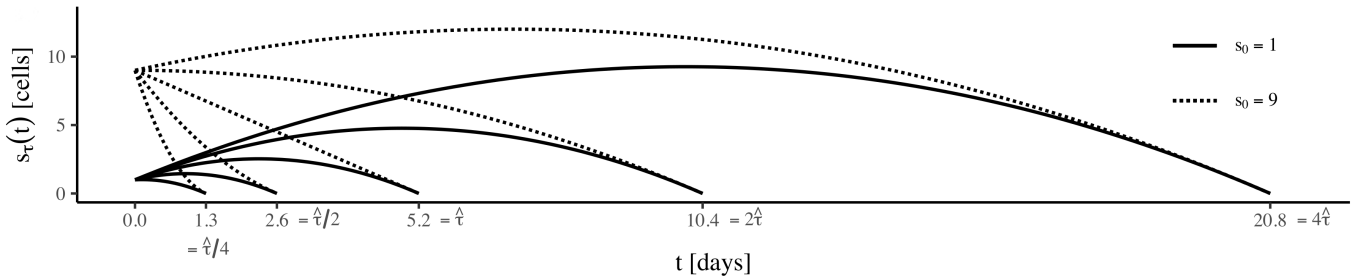


Figure 3. Theoretical extinction trajectories for initial population sizes  $s_0 = 1$  (solid lines) and  $s_0 = 9$  (dotted lines) and different extinction times  $\tau$  (again  $\beta = 4$ ). For  $s_0 = 9$ , the critical time is  $\hat{\tau} = 5.2$ , and the different trajectories exhibit the *sub-linear*, *superlinear* and *initial growth* cases explained in the main text. The larger the extinction time  $\tau$ , the more do the trajectories for  $s_0 = 1$  and  $s_0 = 9$  approach one another for large  $t$ . This demonstrates, that in the critical state the trajectories are dominated by stochasticity, and hence obtain a universal form independent of the initial conditions.

scale of growth vanishes ( $\alpha = 0$ ) and growth is fully determined by the stochasticity of the process. This is in contrast to many other examples of organ growth and regeneration [25–27] where the growth process is arrested in a coordinated manner. An important feature of critical growth is that the long term dynamics of large lineages, which make up most of the organoid, does not depend on the initial conditions of the process. Here stochastic fluctuations have erased all memory of the lineage’s initial size. This might hint at a biological advantage of the critical regime: the outcome of the growth process is less influenced by perturbations in its initial stages, when the tissue is most susceptible to disturbances.

Second, the critical nature of the process implies a mechanism balancing the rates of division and differentiation of stem cells. Such balancing mechanisms are known from homeostatic stem cell renewal [28]. One distinguishes between mechanisms based on asymmetric division (only one daughter cell is a stem cell while the other differentiates) and population asymmetry (the rates of stem cell loss and division are balanced on population level). The first strategy cannot produce critical lineage dynamics because it is strictly deterministic. On the population level, stem cell niches are a well known regulatory mechanism [7, 29, 30] found in intestinal crypts [29] and the adult human brain [31]. Here, stem cells are packed in niches. The available niche space limits the number of possible divisions and a division within the niche can only occur, if another stem cell is carried outside the niche. Even outside homeostasis (the organoids grow by more than an order of magnitude during the experiment), the competition for a scarce resource, e.g. space or nu-

trients, can provide a feedback loop that limits the stem cells’ ability for division at the population level. Such a feedback loop is often encountered in models of self organized criticality (SOC) [32], where the event probabilities are balanced and tuned to the critical point e.g. by energy conservation. For cerebral tissue, the currently available data gives no clues to the nature of the balancing mechanism. The search, however, could inspire future experimental research. Recent advances in lineage tracing allow to study the spatial distribution of lineages in cerebral organoids using light-sheet microscopy and spatial transcriptome sequencing [33]. Inferring the spatial dynamics of the growth process could help to identify the the mechanism behind organoid SOC. Quantitative lineage tracing experiments with other organoid types such as intestinal [20, 21] or cardiac organoids [18, 19] could reveal whether critical growth is specific to cerebral tissue, or whether it is a more general organizing principle.

## ACKNOWLEDGMENTS

We thank C. Esk, S. Haendeler, B. Jeevanesan, J. F. Karcher, and D. Lindenhofer for inspiring discussions. This project has received funding from the European Union’s Framework Programme for Research and Innovation Horizon 2020 (2014-2020) under the Marie Curie Skłodowska Grant Agreement Nr. 847548 (AvH, EK), and from a Special Research Programme (SFB) of the Austrian Science Fund (FWF), project number F78 P11 (AvH, FP).

- 
- [1] L. Chatzeli and B. D. Simons, *Tracing the dynamics of stem cell fate*, Cold Spring Harbor perspectives in biology **12**, a036202 (2020).
- [2] B. D. Simons and H. Clevers, *Strategies for homeostatic stem cell self-renewal in adult tissues*, Cell **145**, 851 (2011).

- [3] Y. Lin, J. Yang, Z. Shen, J. Ma, B. D. Simons, and S.-H. Shi, *Behavior and lineage progression of neural progenitors in the mammalian cortex*, Current Opinion in Neurobiology **66**, 144 (2021).
- [4] C. Zechner, E. Nerli, and C. Norden, *Stochasticity and determinism in cell fate decisions*, Development **147**,



- dev181495 (2020).
- [5] E. Klingler and D. Jabaudon, *Cortical development: Do progenitors play dice?*, *Elife* **9**, e54042 (2020).
  - [6] A. Llorca, G. Ciceri, R. Beattie, F. K. Wong, G. Diana, E. Serafeimidou-Pouliou, M. Fernandez-Otero, C. Streicher, S. J. Arnold, M. Meyer *et al.*, *A stochastic framework of neurogenesis underlies the assembly of neocortical cytoarchitecture*, *Elife* **8**, e51381 (2019).
  - [7] B. Corominas-Murtra, C. L. Scheele, K. Kishi, S. I. Ellenbroek, B. D. Simons, J. Van Rheenen, and E. Hannezo, *Stem cell lineage survival as a noisy competition for niche access*, *Proceedings of the National Academy of Sciences* **117**, 16969 (2020).
  - [8] Q. Smith, E. Stukalin, S. Kusuma, S. Gerecht, and S. X. Sun, *Stochasticity and spatial interaction govern stem cell differentiation dynamics*, *Scientific reports* **5**, 1 (2015).
  - [9] Y. Kashima, Y. Sakamoto, K. Kaneko, M. Seki, Y. Suzuki, and A. Suzuki, *Single-cell sequencing techniques from individual to multiomics analyses*, *Experimental & Molecular Medicine* **52**, 1419 (2020).
  - [10] D. E. Wagner and A. M. Klein, *Lineage tracing meets single-cell omics: opportunities and challenges*, *Nature Reviews Genetics* **21**, 410 (2020).
  - [11] L. Kester and A. van Oudenaarden, *Single-cell transcriptomics meets lineage tracing*, *Cell stem cell* **23**, 166 (2018).
  - [12] C. Esk, D. Lindenhofer, S. Haendeler, R. A. Wester, F. Pflug, B. Schroeder, J. A. Bagley, U. Elling, J. Zuber, A. von Haeseler *et al.*, *A human tissue screen identifies a regulator of er secretion as a brain-size determinant*, *Science* **370**, 935 (2020).
  - [13] M. A. Lancaster, M. Renner, C.-A. Martin, D. Wenzel, L. S. Bicknell, M. E. Hurler, T. Homfray, J. M. Penninger, A. P. Jackson, and J. A. Knoblich, *Cerebral organoids model human brain development and microcephaly*, *Nature* **501**, 373 (2013).
  - [14] M. A. Lancaster, N. S. Corsini, S. Wolfinger, E. H. Gustafson, A. W. Phillips, T. R. Burkard, T. Otani, F. J. Livesey, and J. A. Knoblich, *Guided self-organization and cortical plate formation in human brain organoids*, *Nature biotechnology* **35**, 659 (2017).
  - [15] J. Kim, B.-K. Koo, and J. A. Knoblich, *Human organoids: model systems for human biology and medicine*, *Nature Reviews Molecular Cell Biology* **21**, 571 (2020).
  - [16] M. Völkner, M. Zschätzsch, M. Rostovskaya, R. W. Overall, V. Busskamp, K. Anastasiadis, and M. O. Karl, *Retinal organoids from pluripotent stem cells efficiently recapitulate retinogenesis*, *Stem cell reports* **6**, 525 (2016).
  - [17] G. Quadrato, T. Nguyen, E. Z. Macosko, J. L. Sherwood, S. Min Yang, D. R. Berger, N. Maria, J. Scholvin, M. Goldman, J. P. Kinney *et al.*, *Cell diversity and network dynamics in photosensitive human brain organoids*, *Nature* **545**, 48 (2017).
  - [18] P. Hoang, J. Wang, B. R. Conklin, K. E. Healy, and Z. Ma, *Generation of spatial-patterned early-developing cardiac organoids using human pluripotent stem cells*, *Nature protocols* **13**, 723 (2018).
  - [19] B. Nugraha, M. F. Buono, L. von Boehmer, S. P. Hoerstrup, and M. Y. Emmert, *Human cardiac organoids for disease modeling*, *Clinical Pharmacology & Therapeutics* **105**, 79 (2019).
  - [20] S. Date and T. Sato, *Mini-gut organoids: reconstitution of the stem cell niche*, *Annual review of cell and developmental biology* **31**, 269 (2015).
  - [21] H. C. Angus, A. G. Butt, M. Schultz, and R. A. Kemp, *Intestinal organoids as a tool for inflammatory bowel disease research*, *Frontiers in Medicine* (334) (2020).
  - [22] F. G. Pflug, S. Haendeler, C. Esk, D. Lindenhofer, J. A. Knoblich, and A. von Haeseler, *Neutral competition within a long-lived population of symmetrically dividing cells shapes the clonal composition of cerebral organoids*, *bioRxiv* (2021).
  - [23] N. G. van Kampen, *Stochastic Processes in Physics and Chemistry*, North Holland (2007). ISBN: 978-0444529657.
  - [24] W. Feller, *Die Grundlagen der Volterraschen Theorie des Kampfes ums Dasein in wahrscheinlichkeitstheoretischer Behandlung*, *Acta Biotheoretica* (11–40) (1939).
  - [25] N. Fausto, *Liver regeneration*, *Journal of hepatology* **32**, 19 (2000).
  - [26] Q. Zeng and W. Hong, *The emerging role of the hippo pathway in cell contact inhibition, organ size control, and cancer development in mammals*, *Cancer cell* **13**, 188 (2008).
  - [27] A. P. Ainslie, J. R. Davis, J. J. Williamson, A. Ferreira, A. Torres-Sanchez, A. Hoppe, F. Mangione, M. B. Smith, E. Martin-Blanco, G. Salbreux *et al.*, *Ecm remodeling and spatial cell cycle coordination determine tissue growth kinetics*, *bioRxiv* (2020).
  - [28] B. D. Simons and H. Clevers, *Strategies for homeostatic stem cell self-renewal in adult tissues* **145**, 851. Publisher: Elsevier.
  - [29] K. A. Moore and I. R. Lemischka, *Stem cells and their niches*, *Science* **311**, 1880 (2006).
  - [30] R. Lin and L. Iacovitti, *Classic and novel stem cell niches in brain homeostasis and repair* **1628**, 327.
  - [31] A. Alvarez-Buylla and D. A. Lim, *For the long run: maintaining germinal niches in the adult brain*, *Neuron* **41**, 683 (2004).
  - [32] S. Zapperi, K. B. Lauritsen, and H. E. Stanley, *Self-organized branching processes: mean-field theory for avalanches*, *Physical review letters* **75**, 4071 (1995).
  - [33] Z. He, A. Maynard, A. Jain, T. Gerber, R. Petri, H.-C. Lin, M. Santel, K. Ly, J.-S. Dupré, L. Sidow *et al.*, *Lineage recording in human cerebral organoids*, *Nature methods* **19**, 90 (2022).
  - [34] C. Tsallis, *Lévy distributions*, *Physics World* **10**, 42 (1997).
  - [35] B. Gnedenko and A. Kolmogorov, *Limit distributions for sums of independent random variables*, *Am. J. Math* **105** (1954).
  - [36] J.-P. Bouchaud and A. Georges, *Anomalous diffusion in disordered media: statistical mechanisms, models and physical applications*, *Physics reports* **195**, 127 (1990).
  - [37] D. Dürr and A. Bach, *The Onsager-Machlup function as Lagrangian for the most probable path of a diffusion process*, *Communications in Mathematical Physics* **60**, 153 (1978). Publisher: Springer-Verlag.

## SUPPLEMENTARY MATERIAL

### A. Solving the Fokker-Planck equation

All supplementary equations are marked with an ‘‘S’’, while equation numbers without ‘‘S’’ refer to the main text.

#### 1. The characteristic function

The Fokker-Planck equation (2) can be solved in the Fourier domain. After a Fourier transform, Eq. (2) becomes

$$\frac{\partial \tilde{f}(\mathbf{q}, t)}{\partial t} = - \left[ \frac{\beta}{2} q_s^2 + \alpha i q_s + i g_A (N q_n) + \frac{g_A}{2} (N q_n)^2 - g_A q_s (N q_n) \right] \left( i \frac{\partial}{\partial q_s} \right) \tilde{f}(\mathbf{q}, t) \quad (\text{S1})$$

with

$$\tilde{f}(\mathbf{q}, t) = \int d^3x e^{-i\mathbf{q}\cdot\mathbf{x}} f(\mathbf{x}, t), \quad (\text{S2})$$

where  $\mathbf{q} = (s, n)$ . In the following we will drop the factors of  $N$  for notational simplicity and restore them later on with the substitution

$$q_n \rightarrow N q_n. \quad (\text{S3})$$

Let us choose the initial condition

$$f(\mathbf{x}, t = 0) = \delta(s_0 - s) \delta(n), \quad (\text{S4})$$

which corresponds to  $s_0$  S-cells at  $t = 0$ . In Fourier space this initial condition translates to

$$\tilde{f}(\mathbf{q}, t = 0) = e^{-i s_0 q_s}. \quad (\text{S5})$$

Eq. (S1) contains only first order derivatives and can be solved with the method of characteristics. The characteristic equations are

$$\begin{aligned} \frac{\partial t}{\partial \tau} &= 1 \\ \frac{\partial q_s}{\partial \tau} &= \left[ -\alpha q_s + i \frac{\beta}{2} q_s^2 - g_A q_n + i \frac{g_A}{2} q_n^2 - i g_A q_s q_n \right]. \end{aligned} \quad (\text{S6})$$

The first equation is trivial. It is solved by  $t = \tau$ . The second equation is solved by

$$q_s(t) = \frac{1}{\beta} \frac{i\kappa(q_n) (C_1 e^{t\kappa(q_n)} - 1)}{C_1 e^{t\kappa(q_n)} + 1} + \frac{g_A q_n - i\alpha}{\beta} \quad (\text{S7})$$

with

$$\kappa(q_n) = \sqrt{-(g_A q_n - i\alpha)^2 - 2i\beta D(q_n)} \quad (\text{S8})$$

$$D(q_n) = -g_A q_n + i \frac{g_A}{2} q_n^2. \quad (\text{S9})$$

The solution for the Fourier transformed Fokker-Planck equation (S1) is found by solving for the integration constant  $C_1$ :

$$C_1 = \frac{\alpha + \kappa(q_n) + i g_A q_n - i \beta q_s}{\kappa(q_n) - \alpha - i g_A q_n + i \beta q_s} e^{-t\kappa(q_n)}. \quad (\text{S10})$$

The next step is to look for a function of  $C_1$ ,  $G(C_1(q_s, q_n, t))$ , which satisfies

$$G(C_1)|_{t=0} = q_s, \quad (\text{S11})$$

so that a function  $\tilde{f}(\mathbf{q}, t)$  that satisfies the initial condition of Eq. (S 5) can be written as

$$\tilde{f}(\mathbf{q}, t) = e^{-is_0 G(C_1)}. \quad (\text{S } 12)$$

Such a function is given by

$$\begin{aligned} G(q_s, q_n, t) &= \frac{q_s \rho(q_n, t) - \frac{2}{\beta} \lambda(q_n, t) D(q_n)}{1 + i\lambda(q_n, t) q_s} \\ \lambda(q_n, t) &= \frac{\beta}{\kappa(q_n) \coth\left(\frac{1}{2}\kappa(q_n)t\right) - \alpha - ig_A q_n} \\ \rho(q_n, t) &= \frac{\kappa(q_n) \coth\left(\frac{1}{2}\kappa(q_n)t\right) + \alpha + ig_A q_n}{\kappa(q_n) \coth\left(\frac{1}{2}\kappa(q_n)t\right) - \alpha - ig_A q_n}. \end{aligned} \quad (\text{S } 13)$$

The function  $\tilde{f}(\mathbf{q}, t)$  of Eq. (S 12) is the characteristic function of  $f(\mathbf{x}, t)$ . For later purposes we want to separate  $\kappa(q_n)$  into real and imaginary parts. We find

$$\text{Re}(\kappa(q_n)) = \sqrt{\frac{\sqrt{4g_A^2 q_n^2 (\alpha + \beta)^2 + (\alpha^2 + g_A q_n^2 (\beta - g_A))^2} - g_A^2 q_n^2 + \beta g_A q_n^2 + \alpha^2}{2}} \quad (\text{S } 14)$$

$$\text{Im}(\kappa(q_n)) = \text{sign}(q_n) \sqrt{\frac{\sqrt{4g_A^2 q_n^2 (\alpha + \beta)^2 + (\alpha^2 + g_A q_n^2 (\beta - g_A))^2} + g_A^2 q_n^2 - \beta g_A q_n^2 - \alpha^2}{2}}. \quad (\text{S } 15)$$

## 2. Large $t$ limit. Distribution of $N$ cells.

Let us gain some intuition into the dynamics of the growth process. If the S-cells are dividing at a near critical near zero rate  $\alpha$ , while they are differentiating at a much larger rate  $g_A$ , we can expect that, as  $t$  grows, most lineages will consist of differentiated cells. Lineages that escaped differentiation will have to be very lucky and sufficiently large. As a first step, we want to consider the distribution differentiated cells.

The inverse Fourier transform of Eq. (S 12) with respect to  $q_s$  reads

$$f(s, q_n, t) = \int \frac{dq_s}{2\pi} e^{iq_s s - is_0 G(q_s, q_n, t)}. \quad (\text{S } 16)$$

This expression can be rewritten as

$$\begin{aligned} f(s, q_n, t) &= e^{-\frac{\rho s_0}{\lambda}} \int \frac{dq_s}{2\pi} e^{iq_s s} \left[ \exp\left(\frac{is_0 2D(q_n) \lambda / \beta + \rho s_0 / \lambda}{1 + i\lambda q_s}\right) - 1 + 1 \right] \\ &= e^{-\frac{\rho s_0}{\lambda}} \int \frac{dq_s}{2\pi} e^{iq_s s} \left[ \exp\left(\frac{is_0 2D(q_n) \lambda / \beta + \rho s_0 / \lambda}{1 + i\lambda q_s}\right) - 1 \right] + e^{-\frac{\rho s_0}{\lambda}} \delta(x_s). \end{aligned} \quad (\text{S } 17)$$

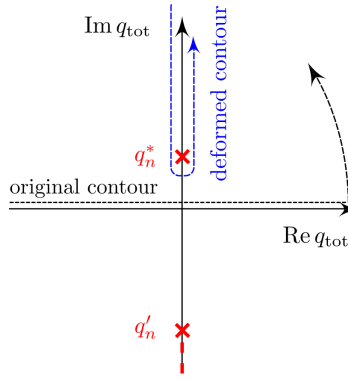
We have thus separated the function  $f(x_s, q_n, t)$  into a part which depends on  $x_s$  and describes lineages that are still evolving and a second part with  $x_s = 0$ . This latter part contains information on the distribution of N-cells in fully differentiated lineages. Its inverse Fourier transform with respect to  $q_n$  is given by

$$f(s=0, n) = e^{-\frac{\alpha}{\beta} s_0} \int \frac{dq_n}{2\pi} \exp\left(iq_n \left(n - s_0 \frac{g_A}{\beta}\right) - s_0 \frac{\kappa(q_n)}{\beta}\right) \quad (\text{S } 18)$$

Notice that  $f(s=0, n)$  does not depend on time. We will later see that  $f(s=0, n)$  is the  $t \rightarrow \infty$  limit of the distribution of total lineage sizes (see Eq. (4) in the main text). Note that the integrand of the first right hand side term in the second line of Eq. (S 17) approaches zero as  $q_s \rightarrow \infty$ . This is a consequence of separating out the delta function and is necessary to regularize the integral. We will attend to this issue below. To do the integral in Eq. (S 18), it is useful to take a look at the analytic structure of the integrand. Nonanalyticities arise from the square root structure of  $\kappa(q_n)$ . Two branch cuts start at the two imaginary roots of  $\kappa(q_n)$  and run to  $+\infty$  and  $-\infty$  along the imaginary  $q_n$  axis (see Fig. S 1). The positive imaginary root is

$$iq_n^* \equiv \frac{i\alpha^2}{g_A(\alpha + \beta) + \sqrt{\beta g_A(\alpha^2 + 2\alpha g_A + \beta g_A)}}, \quad (\text{S } 19)$$





Supplementary Figure S 1. The branch-cut and contour integration in Eq. (S23).

while for the negative imaginary root we find

$$iq_n' = \frac{i\alpha^2}{g_A(\alpha + \beta) - \sqrt{\beta g_A(\alpha^2 + 2\alpha g_A + \beta g_A)}}. \quad (\text{S20})$$

For small  $|\alpha| \ll \beta$ , we have

$$iq_n^* \approx \frac{i\alpha^2}{2\beta g_A}, \quad (\text{S21})$$

$$iq_n' \approx -\frac{2i\beta}{\beta - g_A} - \frac{2i\alpha}{\beta - g_A}. \quad (\text{S22})$$

We thus make a crucial observation: The branch-cut in the upper complex half-plane of  $q_n$  descends to the origin for  $\alpha = 0$ , while the branch cut in the lower half plane always starts below  $-2i\beta/(\beta - g_A)$ . For  $n > 0$ , the integral over the real line in the inverse Fourier transform in Eq. (S18) can be deformed to an integral around the branch cut running from  $+i\infty$  to  $q_n^*$  to the left hand side of the branch cut (at a small distance  $\varepsilon$ , say), and then running back to infinity on the right hand side (see Fig. S 1). The half-circle around  $q_n^*$  is of order  $\varepsilon$  and can be neglected. We can write

$$\begin{aligned} f(s=0, n) &= e^{-\frac{\alpha s_0}{\beta}} \int \frac{dq_n}{2\pi} \exp \left\{ iq_n \left( n - s_0 \frac{g_A}{\beta} \right) - s_0 \frac{\kappa(q_n)}{\beta} \right\} \\ &= e^{-\frac{\alpha s_0}{\beta}} \int_{\infty}^{q_n^*} \frac{idq_n}{2\pi} \exp \left\{ -(q_n - i\varepsilon) \left( n - s_0 \frac{g_A}{\beta} \right) - s_0 \frac{\kappa(iq_n + \varepsilon)}{\beta} \right\} \\ &\quad + e^{-\frac{\alpha s_0}{\beta}} \int_{q_n^*}^{\infty} \frac{idq_n}{2\pi} \exp \left\{ -(q_n + i\varepsilon) \left( n - s_0 \frac{g_A}{\beta} \right) - s_0 \frac{\kappa(iq_n - \varepsilon)}{\beta} \right\}, \end{aligned} \quad (\text{S23})$$

On the new contour, we need

$$\kappa(iq_n) = \sqrt{(\alpha - g_A q_n)^2 - \beta g_A q_n (q_n + 2)}. \quad (\text{S24})$$

It is clear from Eq. (S23) that the most important contribution to the integrals will come from the vicinity of  $q_n^*$ , because the integrand decays exponentially for larger  $q_n$  the faster, the larger  $n$ . Expanding  $\kappa(iq_n)$  around  $q_n^*$ , we obtain

$$\kappa(iq_n \pm \varepsilon) = \pm i \sqrt{2\sqrt{\beta g_A(2\alpha g_A + \alpha^2 + \beta g_A)}(q - q_n^*)} \quad (\text{S25})$$

(approaching the branch cut from different sides changes the sign of the square root). Thus, for large  $n$ , we approximate

Eq. (S23) as

$$\begin{aligned}
f(s=0, n) &\approx -e^{-\frac{\alpha s_0}{\beta}} \int_{q_n^*}^{\infty} \frac{idq_a}{2\pi} \exp \left\{ -q_n \left( n - s_0 \frac{g_A}{\beta} \right) - \frac{s_0}{\beta} i \sqrt{2\sqrt{\beta g_A (2\alpha g_A + \alpha^2 + \beta g_A)} (q_n - q_n^*)} \right\} \\
&\quad + e^{-\frac{\alpha s_0}{\beta}} \int_{q_n^*}^{\infty} \frac{idq_a}{2\pi} \exp \left\{ -q_n \left( n - s_0 \frac{g_A}{\beta} \right) + \frac{s_0}{\beta} i \sqrt{2\sqrt{\beta g_A (2\alpha g_A + \alpha^2 + \beta g_A)} (q_n - q_n^*)} \right\} \\
&= -ie^{-\frac{\alpha s_0}{\beta}} \int_0^{\infty} \frac{dq_a}{2\pi} \exp \left\{ -(q_n + q_n^*) \left( n - s_0 \frac{g_A}{\beta} \right) - \frac{s_0}{\beta} i \sqrt{2pq_n} \right\} \\
&\quad + ie^{-\frac{\alpha s_0}{\beta}} \int_0^{\infty} \frac{dq_a}{2\pi} \exp \left\{ -(q_n + q_n^*) \left( n - s_0 \frac{g_A}{\beta} \right) + \frac{s_0}{\beta} i \sqrt{2pq_n} \right\} \\
&= 2\text{Im} \left( e^{-\frac{\alpha s_0}{\beta}} \int_0^{\infty} \frac{dq_a}{2\pi} \exp \left\{ -(q_n + q_n^*) \left( n - s_0 \frac{g_A}{\beta} \right) + \frac{s_0}{\beta} i \sqrt{2pq_n} \right\} \right) \tag{S26}
\end{aligned}$$

with

$$p = \sqrt{\beta g_A (2\alpha g_A + \alpha^2 + \beta g_A)} \tag{S27}$$

For the remaining integral we obtain

$$\begin{aligned}
f(s=0, n) &\approx \frac{s_0 \sqrt{p} e^{-\frac{-ps_0^2}{2\beta^2(n-s_0\frac{g_A}{\beta})} - q_n^*(n-s_0\frac{g_A}{\beta})}}{\sqrt{2\pi}\beta \left(n - s_0\frac{g_A}{\beta}\right)^{3/2}} \\
&\approx \frac{s_0 \sqrt{p} e^{-q_n^*(n-s_0\frac{g_A}{\beta})}}{\sqrt{2\pi}\beta \left(n - s_0\frac{g_A}{\beta}\right)^{3/2}} \tag{S28}
\end{aligned}$$

This is a truncated, one-sided Lévy distribution [34–36]. The appearance of the Lévy distribution could have been anticipated, since the integrand of Eq. (S18) for  $\alpha = 0$  can be mapped to the characteristic function of the Lévy distribution after the argument of the square root in  $\kappa(q_n)$  has been expanded for small  $q_n$ . For small  $\alpha$  and  $g_0$  we find  $g_A = (-\alpha + \beta - g_0)/2 \approx \beta/2$ , as well as  $p \approx \beta^2/2$ , and for  $n \gg 1$  the truncated power law of Eq. (S28) becomes Eq. (5) of the main text with  $N = 1$ . In the main text, we stated that the  $t \rightarrow \infty$  limit of  $f_{\text{tot}}(x_{\text{tot}}, t)$  – the distribution of total lineage sizes  $x_{\text{tot}}$  – is governed by the same expression as  $f(s=0, n)$  (see Eq. (5) of the main text). We will justify this statement below. On an intuitive level this can be understood as a consequence of the fact that, as  $t$  increases, most cells will already have differentiated and  $f_{\text{tot}}$  will be dominated by the N-cell distribution.

Since  $q_n^*$  descends to the origin as  $\alpha \rightarrow 0$ , the truncation of the 3/2-power-law of (S28) vanishes and (S28) becomes a true Lévy stable power-law distribution. Returning to the observation that the integrand of (S18) is nonanalytic in the lower complex half plane, we conclude that  $f(s=0, n)$  is finite for  $n < 0$ , meaning that there is a finite probability to find a negative number of N-cells. This is a consequence of approximating the discrete master equation by a continuous Fokker-Planck equation which is accurate for large  $s$  and  $n$ . However, one can easily convince oneself that  $f(s=0, n)$  decays very fast as  $n$  decreases below zero: Following the reasoning of the above branch-cut integration, we see that  $f(s=0, n)$  will be suppressed by an exponential factor  $e^{-q_n' n}$ . On the other hand, we see from Eq. (S22) that for small  $\alpha$

$$|q_n'| \gg |q_n^*| \tag{S29}$$

holds. Thus we conclude that the probability for a negative  $n$  is very small, and can be neglected as an artifact of the Fokker-planck approximation. Notice that the probability for negative  $s$  is zero, because Eq. (S12) is analytic in  $q_s$ , except for a single pole which is always in the upper complex half plane (since  $\text{Re}(\lambda(q_n)) > 0$ ) as Eqs. (S14), (S13) indicate). Indeed, while the diffusion coefficient associated with the second derivative in  $s$  in Eq. (3) vanishes at  $s = 0$ , the diffusion coefficient associated with  $n$ -diffusion does not vanish at the origin and allows for a small leakage of probability towards negative  $n$ .

So far we have been investigating the analytic structure of the  $s = 0$  contribution to  $\tilde{f}(\mathbf{q}, t)$ . However similar arguments carry over to the general case. Multiplying the numerator and denominator of the function  $G(q_s, q_n, t)$  in Eq. (S13) by  $\lambda(q_n, t)^{-1}$  and keeping  $q_s$  real for the moment, we see, that the characteristic function  $\tilde{f}(\mathbf{q}, t)$  (Eq. (S12)) is analytic in  $q_n$  except for the branch-cuts of  $\kappa(q_n)$  and the pole at  $\lambda(q_n, t) = i/q_s$ . This pole occurs when

$\lambda(q_n, t)$  is purely imaginary.  $f(s, n, t)$  will decay for  $n < 0$  the faster, the lower the nonanalyticities with  $\text{Im}(q_n) < 0$  lie in the complex plane. Eq. (S 29) shows that the contribution of the lower half branch-cut is indeed negligible since it starts much further away from the origin than the upper branch-cut. A numerical inspection of  $\lambda(q_n, t)$  shows that regions where  $\lambda(q_n, t)$  is purely imaginary in the lower complex half plane of  $q_n$  are indeed sufficiently far from the origin for all reasonable parameter choices. We conclude that the finite values of  $f(s, n, t)$  for negative  $n$  are simply an artifact of the Fokker-Planck approximation to the original master equation (1) and are small.

### 3. The lineage size distribution $f_{\text{tot}}(x_{\text{tot}}, t)$

As pointed out in the main text, we are ultimately interested in the distribution of the lineage size

$$x_{\text{tot}} = s + n. \quad (\text{S } 30)$$

This distribution is obtained by summing  $f(s, n, t)$  over all states which satisfy the condition (S 30):

$$f_{\text{tot}}(x_{\text{tot}}, t) = \int_0^{x_{\text{tot}}} f(s, x_{\text{tot}} - s, t) ds \quad (\text{S } 31)$$

(see also Eq. (4) in the main text). Having argued in Sec. Supplementary Sec. A 2, that the distribution  $f(s, n, t)$  corresponding to the characteristic function (S 12) is confined to positive  $s$  and – to a good approximation – to positive  $n$ , we can extend the integration in Eq. (S 31) to the complete real axis:

$$f(x_{\text{tot}}, t) \approx \int_{-\infty}^{\infty} ds f(s, x_{\text{tot}} - s, t).$$

A Fourier transform then gives

$$\tilde{f}(q_{\text{tot}}, t) \approx \tilde{f}(q_s = q_{\text{tot}}, q_n = q_{\text{tot}}, t), \quad (\text{S } 32)$$

where the characteristic function of Eq. (S 12) is on the right hand side. This yields

$$\tilde{f}(q_{\text{tot}}, t) = \exp\left(\frac{q_{\text{tot}} s_0 [\alpha + 2g_A + \kappa(q_{\text{tot}}) \coth(\frac{1}{2}\kappa(q_{\text{tot}})t)]}{-i\alpha + g_A q_{\text{tot}} - \beta q_{\text{tot}} + i\kappa(q_{\text{tot}}) \coth(\frac{1}{2}\kappa(q_{\text{tot}})t)}\right). \quad (\text{S } 33)$$

*Analytic expressions for the power-law and avalanche regimes* The characteristic function given in Eq. (S 33) has a peculiar behavior at  $q_{\text{tot}} = 0$  which determines the asymptotics for large  $x_{\text{tot}}$ . To see this, let us first investigate the  $t \rightarrow \infty$  and the  $q_{\text{tot}} \rightarrow \infty$  limits of  $\tilde{f}(q_{\text{tot}}, t)$ . Since  $\text{Re}\kappa(q_{\text{tot}}) > 0$  holds for all real  $q_{\text{tot}}$  (see Eq. (S 14)) and  $\text{Re}\kappa(q_{\text{tot}}) \sim |q_{\text{tot}}|$  for large arguments, the approximation

$$\coth\left(\frac{1}{2}\kappa(q_{\text{tot}})t\right) \sim 1 + 2e^{-\kappa(q_{\text{tot}})t} \quad (\text{S } 34)$$

holds in both, the  $t \rightarrow \infty$  and the  $q_{\text{tot}} \rightarrow \infty$  limits. Using (S 34), Eq. (S 33) can be approximated by

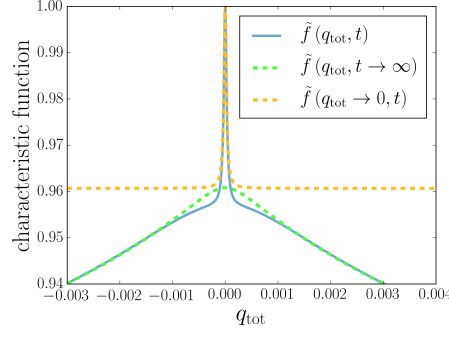
$$\tilde{f}(q_{\text{tot}} \rightarrow \infty, t) \approx \tilde{f}(q_{\text{tot}}, t \rightarrow \infty) \approx \exp\left(-s_0 \frac{ig_A q_{\text{tot}} + \alpha + \kappa(q_{\text{tot}})}{\beta}\right). \quad (\text{S } 35)$$

For  $\alpha > 0$ , this expression approaches  $\exp(-2\alpha s_0/\beta)$  as  $q_{\text{tot}} \rightarrow 0$ , whereas for  $\alpha \leq 0$ , it approaches unity. For the full characteristic function, however,  $\tilde{f}(q_{\text{tot}}, t) = 1$  is true in all cases. This is depicted in Fig. S 2. We conclude that Eq. (S 35) is not a good approximation for small  $|q_{\text{tot}}|$  if  $\alpha > 0$  holds. To find an approximation for small  $|q_{\text{tot}}|$  and positive growth rates, we expand the numerator and denominator inside the exponential function in Eq. (S 33) around  $q_{\text{tot}} \approx 0$  and find

$$q_{\text{tot}} s_0 \left[ \alpha + 2g_A + \kappa(q_{\text{tot}}) \coth\left(\frac{1}{2}\kappa(q_{\text{tot}})t\right) \right] \approx q_{\text{tot}} s_0 \left[ \alpha + 2g_A + |\alpha| \coth\left(\frac{|\alpha|t}{2}\right) \right]$$

and

$$-i\alpha + g_A q_{\text{tot}} - \beta q_{\text{tot}} + i\kappa(q_{\text{tot}}) \coth\left(\frac{1}{2}\kappa(q_{\text{tot}})t\right) \approx i \left( |\alpha| \coth\left(\frac{|\alpha|t}{2}\right) - \alpha \right) + \frac{q_{\text{tot}} \Xi(t)}{2|\alpha|},$$



Supplementary Figure S 2. The full characteristic function  $\tilde{f}(q_{\text{tot}}, t)$  of Eq. (S33) and the approximations for  $t \rightarrow \infty$  or large  $q_{\text{tot}}$ ,  $\tilde{f}(q_{\text{tot}}, t \rightarrow \infty)$ , (Eq. (S35)), as well as for small  $q_{\text{tot}}$ ,  $\tilde{f}(q_{\text{tot}} \rightarrow 0, t)$ , (Eq.S36). We used a positive growth rate  $\alpha = 0.2/\text{day}$  and  $\beta = 10/\text{day}$ . For  $\alpha > 0$  and large but finite  $t$ ,  $\tilde{f}(q_{\text{tot}}, t \rightarrow \infty)$  (green dashed curve) is a good approximation to the characteristic function  $\tilde{f}(q_{\text{tot}}, t)$  (blue curve), except for a small region near  $q_{\text{tot}} = 0$  which is well approximated by  $\tilde{f}(q_{\text{tot}} \rightarrow 0, t)$  (orange curve). This region governs the behavior at large lineage sizes  $x_{\text{tot}}$ .

where

$$\begin{aligned} \Xi(t) &= \text{csch}^2\left(\frac{|\alpha|t}{2}\right) \left[ |\alpha|(\beta + g_A(t(\alpha + \beta) - 1)) - g_A(\alpha + \beta) \sinh(|\alpha|t) + |\alpha|(g_A - \beta) \cosh(|\alpha|t) \right] \\ &\approx -\beta^2 \coth\left(\frac{|\alpha|t}{2}\right) \end{aligned}$$

In the last line we assumed that  $|\alpha| \ll \beta$ . Therefore, the appropriate approximation for  $\alpha > 0$  and small  $|q_{\text{tot}}|$  reads

$$\tilde{f}(q_{\text{tot}} \rightarrow 0, t) \approx \exp\left(\frac{q_{\text{tot}}s_0 \left[ \alpha + 2g_A + |\alpha| \coth\left(\frac{|\alpha|t}{2}\right) \right]}{i \left( |\alpha| \coth\left(\frac{|\alpha|t}{2}\right) - \alpha \right) + \frac{q_{\text{tot}}\Xi(t)}{2|\alpha|}}\right). \quad (\text{S36})$$

It remains to determine the distribution function  $f(x_{\text{tot}}, t)$ . At small and intermediate  $x_{\text{tot}}$ , we expect  $f(x_{\text{tot}}, t)$  to be governed by the behavior of the characteristic function at larger  $q_{\text{tot}}$ , whereas the behavior of  $f(x_{\text{tot}}, t)$  for large  $x_{\text{tot}}$  will be determined by the region around  $q_{\text{tot}} \approx 0$ . This has to do with the analytic structure of Eq. (S33). The question is, which nonanalyticity dominates the Fourier transform as the integration contour is deformed according to Fig. S 1. Besides the branch-cuts of  $\kappa(q_n)$ ,  $\tilde{f}(q_{\text{tot}}, t)$  exhibits a pole on the imaginary axis (see Fig. S 3). Let this pole be located at  $q_{\text{tot}} = iq_{\text{tot}}^*$ . If it is closer to the origin than the upper starting point of the branch-cut, i.e.  $q_{\text{tot}}^* < q_n^*$ , where  $q_n^*$  is defined in Eq. (S19), the pole becomes dominant at large  $x_{\text{tot}}$ . This is because both nonanalyticities, the branch cut starting at  $q_n^*$  and the pole at  $q_{\text{tot}}^*$ , are located on the positive imaginary axis. Hence, when the integration along the deformed contour is performed, the contributions of the pole and the branch-cut will roughly behave as  $e^{-q_{\text{tot}}^*x_{\text{tot}}}$ , or  $e^{-q_n^*x_{\text{tot}}}$ , respectively. We can use Eq. (S36) to track the behavior of  $q_{\text{tot}}^*$  for different parameter values:

$$iq_{\text{tot}}^* = \frac{-2i|\alpha|}{\Xi(t)} \left( |\alpha| \coth\left(\frac{|\alpha|t}{2}\right) - \alpha \right) \approx 2i \frac{\alpha^2}{\beta^2} \left( 1 - \text{sign}(\alpha) \tanh\left(\frac{|\alpha|t}{2}\right) \right). \quad (\text{S37})$$

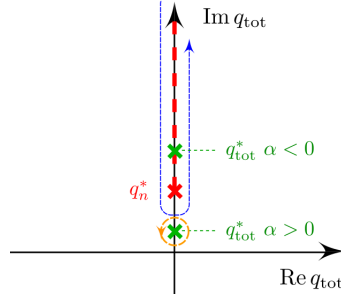
Eq. (S37) shows that the analytic structure of the characteristic function is very different for positive and negative  $\alpha$ . For positive  $\alpha$ , it is  $q_{\text{tot}}^* < q_n^*$ , and therefore  $f(x_{\text{tot}}, t)$  will be dominated by the single pole that is captured in Eq. (S37). For  $\alpha < 0$ , the opposite scenario is true: we find  $q_n^* < q_{\text{tot}}^*$ .

We now calculate the inverse Fourier transforms Eqs. (S35) and (S36) which will give us approximate expressions for  $f(x_{\text{tot}}, t)$  at intermediate and large  $x_{\text{tot}}$ . The inverse Fourier transform of Eq. (S35) reads

$$f_{\text{tot}}^{t \rightarrow \infty}(x_{\text{tot}}) \equiv \int \frac{dq_{\text{tot}}}{2\pi} e^{iq_{\text{tot}}x_{\text{tot}}} \lim_{t \rightarrow \infty} \tilde{f}(q_{\text{tot}}, t) = e^{-\frac{\alpha}{\beta}s_0} \int \frac{dq_n}{2\pi} \exp\left(iq_{\text{tot}} \left(x_{\text{tot}} - s_0 \frac{g_A}{\beta}\right) - s_0 \frac{\kappa(q_{\text{tot}})}{\beta}\right). \quad (\text{S38})$$

We encountered this integral when we calculated the distribution of N-cells in Eq. (S18). Similarly to Eq. (S28) we find

$$f_{\text{tot}}^{t \rightarrow \infty}(x_{\text{tot}}) = \frac{s_0 \sqrt{p} e^{\frac{-ps_0^2}{2\beta^2(x_{\text{tot}} - s_0 \frac{g_A}{\beta})} - q_{\text{tot}}^*(x_{\text{tot}} - s_0 \frac{g_A}{\beta})}}{\sqrt{2\pi}\beta \left(x_{\text{tot}} - s_0 \frac{g_A}{\beta}\right)^{3/2}} \quad (\text{S39})$$



Supplementary Figure S 3. Branch-cut integration (see Fig. S 1 and Eq. (S 23)) and the pole at  $q_{\text{tot}}^*$  (Eq. (S 37)) characterizing the avalanche part of the distribution. Both, the pole and the branch-cut must be captured by the deformed contour (blue dashed line). For  $\alpha > 0$ , the pole at  $q_{\text{tot}}^*$  is always nearer to the origin than the starting point of the branch-cut  $q_n^*$  and thus determines the large  $x_{\text{tot}}$  behavior. For  $\alpha < 0$ ,  $q_{\text{tot}}^*$  is within the integration contour, moving towards larger imaginary values as  $t$  is increased. For sufficiently small  $t$ , the avalanche part of the distribution is still well approximated by the integration around the  $q_{\text{tot}}^*$  pole (see Fig. 2 b)).

with

$$p = \sqrt{\beta g_A (2\alpha g_A + \alpha^2 + \beta g_A)}$$

$$q_n^* = \frac{\alpha^2}{g_A (\alpha + \beta) + \sqrt{\beta g_A (\alpha^2 + 2\alpha g_A + \beta g_A)}}.$$

In order to account for the  $N$  N-cells that each S-cell is producing we have to make the substitution  $q_n \rightarrow Nq_n$  in Eq. (S 32). This substitution carries over to Eq. (S 35) where we have to replace  $q_{\text{tot}}$  by  $Nq_{\text{tot}}$ . The integration of Eq. (S 38) is evaluated according to

$$\int \frac{dq_{\text{tot}}}{2\pi} e^{iq_{\text{tot}}x_{\text{tot}}} \lim_{t \rightarrow \infty} \tilde{f}(Nq_{\text{tot}}, t) = \int \frac{dq'_{\text{tot}}}{N2\pi} e^{iq'_{\text{tot}}x_{\text{tot}}/N} \lim_{t \rightarrow \infty} \tilde{f}(q'_{\text{tot}}, t) = \frac{1}{N} f_{\text{tot}}^{t \rightarrow \infty}(x_{\text{tot}}/N). \quad (\text{S 40})$$

For  $|\alpha| \ll \beta$ , we obtain the result of Eq. (5), Sec. of the main text:

$$f_{\text{tot}}^{t \rightarrow \infty}(x_{\text{tot}}) \approx \frac{s_0 \beta e^{-\frac{\alpha^2 x_{\text{tot}}}{\beta^2 N}}}{2\sqrt{2\pi} N (x_{\text{tot}}/N)^{3/2}}. \quad (\text{S 41})$$

According to the above discussion, Eq. (S 41) is valid for intermediate  $x_{\text{tot}}$  if  $\alpha > 0$ . For  $\alpha < 0$ , the contribution of the pole becomes stronger and stronger sub-leading to the branch-cut contribution as  $t$  is increased (see Eq. (S 37)). However, if  $t$  is sufficiently small, the pole is in the vicinity of the branch-cut starting point  $q_n^*$  and has a strong influence on the distribution function. For large enough  $t$  however, Eq. (S 41) is a good approximation for  $f_{\text{tot}}(x_{\text{tot}})$  everywhere.

To determine the behavior at large  $x_{\text{tot}}$  for  $\alpha > 0$  we make use of Eq. (S 36) which gives a good approximation for the characteristic function at small  $q_{\text{tot}}$ . It is useful to rewrite Eq. (S 41) as

$$\tilde{f}(q_{\text{tot}} \rightarrow 0, t) = e^{-aq_{\text{tot}}} \exp\left(\frac{aq_{\text{tot}}^*}{1 + iq_{\text{tot}}/q_{\text{tot}}^*}\right)$$

with

$$a = \frac{s_0 (\alpha + 2g_A + \alpha \coth(\frac{\alpha t}{2}))}{\alpha (\coth(\frac{\alpha t}{2}) - 1)}. \quad (\text{S 42})$$

The inverse Fourier transform

$$f_{\text{tot}}(x_{\text{tot}} \rightarrow \infty, t) = e^{-aq_{\text{tot}}} \int \frac{dq_{\text{tot}}}{2\pi} \exp\left(iq_{\text{tot}}x_{\text{tot}} + \frac{aq_{\text{tot}}^*}{1 + iq_{\text{tot}}/q_{\text{tot}}^*}\right) \quad (\text{S 43})$$

is strictly speaking divergent (as is the one in Eq. (S 17)). However it can be regularized by adding a small exponential factor  $e^{-q_{\text{tot}}|\epsilon|}$  to the integrand and letting  $\epsilon \rightarrow 0$  after the integral is done. The large  $x_{\text{tot}}$  behavior that we are

interested in is dominated by the pole at  $q_{\text{tot}}^*$  for  $\alpha > 0$ . We will see later, that for  $\alpha < 0$ , the pole still dominates the distribution for reasonably large  $x_{\text{tot}}$  (avalanche regime) if  $t$  is small, although it does not govern the asymptotics for  $x_{\text{tot}} \rightarrow \infty$ . The pole's contribution can be found by integrating along a circle around  $q_{\text{tot}}^*$  (see Fig. S 3). Writing

$$q_{\text{tot}} = iq_{\text{tot}} + re^{i\varphi}$$

the integral around the pole at  $q_{\text{tot}}$  becomes

$$f_{\text{tot}}(x_{\text{tot}} \rightarrow \infty, t) = \exp\left(-\frac{a}{q_{\text{tot}}} - \frac{x_{\text{tot}}}{q_{\text{tot}}}\right) ir \int_0^{2\pi} \frac{e^{i\varphi} d\varphi}{2\pi} \exp\left(ir e^{i\varphi} x_{\text{tot}} + \frac{a}{iq_{\text{tot}}^2 r e^{i\varphi}}\right).$$

Since the radius  $r$  is arbitrary, we are free to chose

$$r = \sqrt{\frac{a}{q_{\text{tot}}^2 x_{\text{tot}}}}.$$

After some algebra, we arrive at

$$f_{\text{tot}}(x_{\text{tot}} \rightarrow \infty, t) = \exp\left(-\frac{a}{q_{\text{tot}}} - \frac{x_{\text{tot}}}{q_{\text{tot}}}\right) r \int_0^{2\pi} \frac{e^{i\varphi} d\varphi}{2\pi} \exp\left(rx_{\text{tot}} \left[e^{i\varphi} + \frac{1}{e^{i\varphi}}\right]\right). \quad (\text{S 44})$$

Using the integral representation of Bessel functions

$$I_n(z) = \frac{1}{2\pi i} \int_{\mathcal{C}} dt \frac{e^{\frac{z}{2}(t+\frac{1}{t})}}{t^{n+1}},$$

where  $\mathcal{C}$  is a contour enclosing the origin, with the substitution  $t = e^{i\varphi}$  Eq. (S 44) becomes

$$f_{\text{tot}}(x_{\text{tot}} \rightarrow \infty, t) = \theta(x_s) \exp\left(-\frac{a}{q_{\text{tot}}} - \frac{x_{\text{tot}}}{q_{\text{tot}}}\right) \sqrt{\frac{a}{q_{\text{tot}}^2 x_{\text{tot}}}} I_1\left(2\sqrt{\frac{ax_{\text{tot}}}{q_{\text{tot}}^2}}\right). \quad (\text{S 45})$$

For  $\alpha > 0$ , this is the large  $x_{\text{tot}}$  approximation for the distribution function  $f(x_{\text{tot}}, t)$  given in Eq. (6), where we have restored the variable  $N$ . As is demonstrated in Fig. (2), Eq. (S 45) provides a good approximation for the large  $x_{\text{tot}}$  behavior of  $f_{\text{tot}}(x_{\text{tot}}, t)$  for a positive S-cell growth rate  $\alpha$ . However, even for  $\alpha < 0$ , at reasonably large  $x_{\text{tot}}$  (namely in the avalanche regime), the behavior of the lineage size probability density is well described by Eq. (S 45), if  $\alpha t \lesssim 1$  holds. This is due to the fact that the pole at  $q_n^*$ , while located above  $q_n^*$  on the imaginary  $q_{\text{tot}}$  line (see Fig. S 3), is still sufficiently near  $q_n^*$  to dominate the avalanche part of the distribution function (see Eq. (S 37)). However, the asymptotics of  $f_{\text{tot}}(x_{\text{tot}}, t)$  for  $x_{\text{tot}} \rightarrow \infty$  will not be given by Eq. (S 45). Since in both cases, for positive and negative  $\alpha$ , Eq. (S 45) is an approximation for the avalanche part of the lineage size probability density, we call it  $f_{\text{tot}}^{\text{av.}}(x_{\text{tot}}, t)$ .

## B. Most-likely paths

We now derive the most likely path  $s_\tau(t)$  that a critical S-cell population (i.e.  $\alpha = 0$ ) takes from  $s_0$  cells at  $t = 0$  to extinction at  $t = \tau$ . Since we consider only S-cells and only critical populations, equation (3), according to the rules of Ito's calculus, reduces a process described by the stochastic differential equation (SDE)

$$ds = \sqrt{\beta s} dw(t) \quad (\text{S 46})$$

where  $w(t)$  is the standard Brownian motion. If the set of possible paths was finite-dimensional, we could proceed by finding the density  $W$  defined by equation (S 46) on the set of possible paths starting at  $s_0$  and maximizing  $W(s_\tau)$  subject to  $s_\tau(\tau) = 0$  to find  $s_\tau$ . It turns out, however, that this approach only cleanly generalizes to infinite-dimensional path spaces in the case of a constant diffusion term [37]. To avoid these technical difficulties, we perform a change of variable to transform equation (S 46) into a process with a constant diffusion term. By setting  $y(t) = 2\sqrt{s(t)}/\beta$  and applying Itô's lemma we get

$$dy = A(y)dt + dw(t) \text{ where } A(y) = -\frac{1}{2y} \quad (\text{S 47})$$

(were once  $y$  reaches zero, we define it to remain there, despite  $A$  becoming undefined). For this process, the density functional  $W$  expressed in terms of its Lagrangian  $L$  (also called Onsager-Machlup function) is [37]

$$W[y(t)] \sim e^{-S(y)} \quad (\text{S 48})$$

$$\text{where } S[y] = \frac{1}{2} \int_0^T L(y, \dot{y}) dt$$

$$\text{and } L(y, \dot{y}) = (\dot{y} - A(y))^2 + A'(y).$$

The functional  $W$  defines a probability density on the set of paths in the following sense: The probability for a random path to lie within a small tube of diameter  $\epsilon$  around a given differentiable path  $y$  is asymptotically proportional to  $W[y]H(\epsilon)$  for some function  $H$  independent of  $y$  (this factorization fails if the diffusion term is not constant [37]). We can therefore proceed as we would in the finite-dimensional case and maximize  $W$  to find  $y_\tau$ . Since maximizing  $W$  means minimizing the *action*  $S(y) = \frac{1}{2} \int_0^T L(y, \dot{y}) dt$ , the desired  $y_\tau$  is found by solving the Euler-Lagrange (EL) equation  $\frac{d}{dt} \frac{\partial L}{\partial \dot{y}} = \frac{\partial L}{\partial y}$ . In our case the EL equation yields  $\ddot{y} = -\frac{3}{4}y^{-3}$  with the general solution

$$y(t) = \sqrt{\lambda t^2 + \mu t + \nu} \quad (\text{S 49})$$

$$\text{where } \mu^2 = 4\lambda\nu + 3,$$

and solving for the boundary conditions  $y(0) = u(s_0) = 2\sqrt{s_0/\beta}$  and  $y(\tau) = 0$  yields

$$\nu = s_0 \frac{4}{\beta}, \mu = \sqrt{3} - 2\frac{\nu}{\tau}, \lambda = \frac{1}{\tau} \left( \frac{\nu}{\tau} - \sqrt{3} \right)$$

(where we chose the solution that ensures  $\lambda t^2 + \mu t + \nu \geq 0$  on  $[0, \tau]$ ). Inserting these parameters into the general solution (S 49) and transforming back from  $y$  to  $s$  produces after some rearrangements the extinction trajectory stated in equation (10).